



AFRL-AFOSR-VA-TR-2019-0350

Nonlinearity in the resolvent analysis: recovery of the mean velocity profile and energy transfer paths in wall turbulence

Beverley Mckeon
CALIFORNIA INSTITUTE OF TECHNOLOGY
1200 E. CALIFORNIA BLDV
PASADENA, CA 91125

11/19/2019
Final Report

DISTRIBUTION A: Distribution approved for public release.

Air Force Research Laboratory
AF Office Of Scientific Research (AFOSR)/RTA1

DISTRIBUTION A: Distribution approved for public release.

Arlington, Virginia 22203
Air Force Materiel Command

REPORT DOCUMENTATION PAGE				<i>Form Approved</i> OMB No. 0704-0188	
<p>The public reporting burden for this collection of information is estimated to average 1 hour per response, including the time for reviewing instructions, searching existing data sources, gathering and maintaining the data needed, and completing and reviewing the collection of information. Send comments regarding this burden estimate or any other aspect of this collection of information, including suggestions for reducing the burden, to Department of Defense, Executive Services, Directorate (0704-0188). Respondents should be aware that notwithstanding any other provision of law, no person shall be subject to any penalty for failing to comply with a collection of information if it does not display a currently valid OMB control number.</p> <p>PLEASE DO NOT RETURN YOUR FORM TO THE ABOVE ORGANIZATION.</p>					
1. REPORT DATE (DD-MM-YYYY) 19-11-2019		2. REPORT TYPE Final Performance		3. DATES COVERED (From - To) 01 Sep 2016 to 31 Aug 2019	
4. TITLE AND SUBTITLE Nonlinearity in the resolvent analysis: recovery of the mean velocity profile and energy transfer paths in wall turbulence				5a. CONTRACT NUMBER	
				5b. GRANT NUMBER FA9550-16-1-0361	
				5c. PROGRAM ELEMENT NUMBER 61102F	
6. AUTHOR(S) Beverley Mckeon				5d. PROJECT NUMBER	
				5e. TASK NUMBER	
				5f. WORK UNIT NUMBER	
7. PERFORMING ORGANIZATION NAME(S) AND ADDRESS(ES) CALIFORNIA INSTITUTE OF TECHNOLOGY 1200 E. CALIFORNIA BLDV PASADENA, CA 91125 US				8. PERFORMING ORGANIZATION REPORT NUMBER	
9. SPONSORING/MONITORING AGENCY NAME(S) AND ADDRESS(ES) AF Office of Scientific Research 875 N. Randolph St. Room 3112 Arlington, VA 22203				10. SPONSOR/MONITOR'S ACRONYM(S) AFRL/AFOSR RTA1	
				11. SPONSOR/MONITOR'S REPORT NUMBER(S) AFRL-AFOSR-VA-TR-2019-0350	
12. DISTRIBUTION/AVAILABILITY STATEMENT A DISTRIBUTION UNLIMITED: PB Public Release					
13. SUPPLEMENTARY NOTES					
14. ABSTRACT The present research extended resolvent analysis in canonical turbulent flows to analysis of the nonlinear forcing term. Full characterization of the nonlinear forcing is equivalent to making the formulation self-consistent and self-sustaining. The work provided a rigorous, non-empirical framework to reconstruct the mean velocity profile from an assembly of correctly-weighted resolvent modes, determined weights for individual triadic interactions, and used these results to give new insight for turbulence models. The study included analysis, modeling, experimental excitation of individual triadic interactions using dynamic roughness and investigation of controlled flow.					
15. SUBJECT TERMS resolvent analysis + turbulence, linear resolvent operator + turbulence, self-adjoint operator + turbulence					
16. SECURITY CLASSIFICATION OF:			17. LIMITATION OF ABSTRACT UU	18. NUMBER OF PAGES	19a. NAME OF RESPONSIBLE PERSON ABATE, GREGG
a. REPORT Unclassified	b. ABSTRACT Unclassified	c. THIS PAGE Unclassified			19b. TELEPHONE NUMBER (include area code) 703-588-1779

FINAL REPORT

Grant # FA 9550-16-1-0361

Nonlinearity in the resolvent analysis: recovery of the mean velocity
profile and energy transfer paths in wall turbulence

Beverley J. McKeon
Graduate Aerospace Laboratories
California Institute of Technology
Pasadena, CA 91125

Executive Summary

The ubiquity of wall turbulence, in aerospace applications and elsewhere, has made this phenomenon a topic of study over many decades. Yet it still poses intellectual and practical challenges that preclude rigorous analytical predictive capabilities. In recent work under AFOSR sponsorship, we laid groundwork towards this goal, defining an exact analysis of the Navier-Stokes equations (NSE) for canonical wall turbulence that is amenable to extension to include control and which can be performed without resort to high performance computing (McKeon & Sharma, 2010).

In the present research, we proposed an extension of the resolvent analysis in canonical flows, which had focused on the dynamics of the linear Navier-Stokes operator, to the nonlinear forcing term. The nonlinearity couples turbulent activity at different wavenumbers and frequencies through its quadratic nature, dynamically linking triadically consistent structures and establishing energy transfer paths. Importantly, it also determines the mean velocity profile through the profile of Reynolds stress. Thus, full characterization of the nonlinear forcing in the resolvent analysis is equivalent to making the formulation self-consistent and self-sustaining. Our goals were to provide a rigorous, non-empirical framework to reconstruct the mean velocity profile from an assembly of correctly-weighted resolvent modes, to determine weights for individual triadic interactions, and to use these results to investigate the potential adaptation of resolvent analysis to give new insight into wall and sub-grid scale turbulence models. The study included analysis, modeling and experimental demonstration of the excitation of individual triadic interactions using dynamic roughness, and extending our results from unperturbed to controlled flow.

The structure of the resolvent operator was exploited by using state-of-the-art matrix approximation (randomized approximation) and data reduction techniques to preserve the low calculation overhead, with a view to maintaining the efficiency of the resolvent analysis in comparison with direct simulation.

This research resulted in a series of manuscripts (11 published, 3 under review) pertaining to increasingly sophisticated treatments of nonlinearity in resolvent analysis, recovery and modeling of the mean velocity profile, experimental demonstration of synthetic nonlinear interactions, and the proposal of resolvent analysis as a tool by which to vet the likely efficacy of proposed control strategies at significantly reduced cost relative to either full, direct simulation or experiment.

The work has suggested several avenues for future development, with a view to generating self-sustaining, nonlinear, low-order models of wall turbulence which exploit the mathematical structure of the (spatiotemporal) resolvent to obtain efficient representations of dynamically important flow features.

Contents

1	Introduction and Objectives	4
2	Background	5
3	Summary of Results	6
3.1	Analysis of turbulent flows using resolvent analysis: efficient projections of data onto resolvent modes, characterization of the nonlinear forcing and consistency with the mean velocity profile	6
3.1.1	Resolvent analysis based on the Orr-Sommerfield/Squire decomposition	6
3.1.2	Low-rank capture of linear response and nonlinear forcing in Exact Coherent States (ECS)	7
3.1.3	Convergence to exact coherent solutions starting from the laminar velocity profile . .	8
3.1.4	Optimization of resolvent mode weights in fully-turbulent channel flow	10
3.1.5	Scaling of resolvent mode weights by consideration of mode interactions	13
3.2	Experimental excitation of a triadic interaction	15
3.3	New approaches to turbulence modeling and control	16
3.3.1	Measures of non-normality	16
3.3.2	Coherent structures and uniform momentum zones from resolvent modes	17
3.3.3	Resolvent as a tool to evaluate control technologies - Opposition control example . . .	18
3.3.4	Low-order models of linear and nonlinear effects in wall turbulence	21
3.4	Review articles	22
4	Conclusions and Outlook	23
5	Archival products under this grant	24
6	References	25

1 Introduction and Objectives

The work performed under this grant pertained to the incorporation of nonlinear forcing into the resolvent analysis approach proposed by McKeon & Sharma [1]. The specific objectives of the research, as listed in the original proposal, were as follows.

Extend the resolvent framework from the current (successful) focus on the operator governing the linear dynamics, and the corresponding velocity response, to characterize the nonlinear interactions. These regulate the forcing input, govern the mean velocity profile (currently assumed) and describe how different wavenumber/frequency combinations must interact to reconstruct the full turbulent velocity and pressure fields in incompressible wall turbulence.

To reach this objective, the following individual tasks were proposed.

1. Characterize our existing results concerning scaling of the velocity modes obtained by projecting results from simulation and experiment onto resolvent modes in terms of weights and nonlinear interactions (see section 4.1).
2. Identify and model the key characteristics of the nonlinear forcing term giving rise to the correct Reynolds stress profile, such that the mean velocity is correctly recovered from the analysis (see section 4.2).
3. Identify and model the key characteristics of the triadic resolvent mode interactions governing the nonlinear forcing at specific wavenumber/frequency combinations, such that the system of figure 1 approaches closure (see section 4.3).
4. Use dynamic roughness perturbation to excite a synthetic wavenumber/frequency triad in a canonical turbulent boundary layer and compare measured (phase-lock reconstructed) velocity response with resolvent predictions (see section 4.4).
5. Exploit rules governing permitted nonlinear interactions between wavenumber/frequency triplets to propose new means of modeling wall turbulence near the wall and at small scales, i.e. in terms amenable to description in terms of new wall models and sub-grid scale models (see section 4.5).

It was also proposed to continue to exploit the structure of the resolvent operator, using state-of-the-art matrix approximation and data reduction techniques to preserve the low calculation overhead, with a view to maintaining the efficiency of the resolvent analysis in comparison with direct simulation. We anticipated performing exploratory studies of the feasibility of extending our results from unperturbed flow to non-canonical cases, i.e. under control.

2 Background

The analysis employed in this work is a logical development of the resolvent analysis laid out by McKeon & Sharma [1] for incompressible turbulent flows. The essence of that approach is described in Figure 1. The resolvent is the transfer function between the nonlinear terms in the Navier-Stokes equations, which are treated as a forcing of the linear dynamics, and the linear state response (here indicated in terms of the velocity fluctuations, i.e. for a divergence-free basis, relative to the turbulent mean). The analysis accounts for the amplification of forcing input due to the non-normality of the resolvent [2], which is similar to the linearized Navier-Stokes operator familiar from hydrodynamic stability theory although without the restrictions on the magnitude of the perturbation from the equilibrium (laminar) state. Analysis of the resolvent using a singular value decomposition (SVD) subject to an energy norm at each spatio-temporal scale reveals that it can be approximated in an extremely low-order fashion when there is a physical mechanism extracting energy from the mean flow [3]. Equivalently, the spatio-temporal basis used in the analysis efficiently identifies forcing structure which is preferentially amplified by the resolvent, giving rise to the “most likely observable” response mode shapes at each scale. The analysis can be considered to be the equation-driven equivalent of data analysis techniques such as Proper Orthogonal Decomposition, which require full-field information rather than simply the governing equations [4]. Full details of the analysis will be laid out in the context of compressible turbulent boundary layers in Section 3 below.

Notably, the cost of resolvent analysis is significantly less than high performance computations, since it rests on linear algebra techniques which have been the subject of intensive development in other fields in recent years. For a one-dimensional turbulent mean profile, i.e. a quasi-parallel assumption for a turbulent boundary or a periodic domain for an internal flow, the cost of performing the SVD is so low that analysis can proceed on a laptop computer. More computing power is required for two-dimensional mean flows - with associated data storage limitations which have limited the size of the domain which can be considered - but still at the local core rather than national HPC facility level.

A recent review of resolvent analysis for incompressible wall turbulence and an overview of what can be learned about turbulence structure and self-sustaining mechanisms is given in [5]. The approach has now been used to analyze a wide range of turbulent flow configurations.

In this work, we continue our investigation into resolvent modeling of wall turbulence, focusing on what can be learned about and from the nonlinear interactions between resolvent modes in the pursuit of closure modeling strategies for the loop of Figure 1. The approach taken towards each of the objectives listed in the previous section is described in what follows, grouped by analysis, experiments and modeling directions.

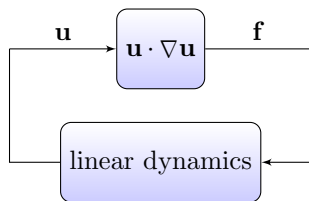


Figure 1: A high-level description of the turbulence process in resolvent analysis. The lower block contains the linear dynamics of the fluctuations interacting with the mean velocity profile. After [1].

3 Summary of Results

An outline of key results and outcomes from the grant is given in this section. The archival manuscripts which give full information are identified (and appended to this report).

3.1 Analysis of turbulent flows using resolvent analysis: efficient projections of data onto resolvent modes, characterization of the nonlinear forcing and consistency with the mean velocity profile

Results from the first three objectives of section 1 are grouped together in this subsection because of a common enabling work. Efforts to find the most efficient resolvent basis for parallel turbulent shear flows are described in terms of:

- an Orr-Sommerfeld/Squire (OS/SQ) decomposition of the resolvent,
- the subsequent extremely low rank projections of exact coherent states (as a proxy for fully turbulent flows) onto the OS/SQ basis, capture of the nonlinear forcing, and consistent recovery of the (assumed) mean profile, and a method to iterate on the weights of resolvent modes to obtain nonlinear, self-sustaining ECS solutions with knowledge of the mean flow (using ECS as a proxy for fully turbulent solutions of the Navier-Stokes equations)
- a method to obtain self-sustaining ECS solutions without prior knowledge of the mean profile, i.e. starting from the analytic, laminar profile and iterating to convergence to a solution,
- low rank projections of fully turbulent channel flow onto the OS/SQ resolvent basis, and
- connection of these projected weights with, and extension of, scaling results for (triadic/resonant) nonlinear resolvent mode interactions.

These results correspond to a increasingly sophisticated set of methods to close the nonlinear loop of Figure 1.

3.1.1 Resolvent analysis based on the Orr-Sommerfeld/Squire decomposition

Rosenberg, K. & McKeon, B. J. Efficient representations of exact coherent states of the Navier-Stokes equations using resolvent analysis Fluid Dyn. Res., 51, 011401 (2019).

The standard resolvent decomposition is optimal in the kinetic energy norm. However, in wall-bounded turbulence the kinetic energy is often dominated by the the streamwise velocity, which means that all three velocity components may not be approximated uniformly well [6, 7]. In such situations, an alternative decomposition that more faithfully represents the underlying dynamics may be desirable. To this end, we proposed [8] an alternative decomposition of \mathcal{H} , which reveals a critical insight about wall turbulence and consequently leads to a more efficient resolvent basis.

The resolvent in velocity-vorticity form for an incompressible turbulent flow with a one-dimensional mean velocity profile, $U(y)$, can be written as

$$\begin{pmatrix} \hat{v} \\ \hat{\eta} \end{pmatrix} = \begin{pmatrix} \mathcal{H}_{vv} & 0 \\ \mathcal{H}_{\eta v} & \mathcal{H}_{\eta\eta} \end{pmatrix} \begin{pmatrix} \hat{g}_v \\ \hat{g}_\eta \end{pmatrix}, \quad (1)$$

where

$$\mathcal{H}_{vv} = (-i\omega - \Delta^{-1}\mathcal{L}^{\text{OS}})^{-1}, \quad (2)$$

$$\mathcal{H}_{\eta\eta} = (-i\omega - \mathcal{L}^{\text{SQ}})^{-1}, \quad (3)$$

$$\mathcal{H}_{\eta v} = -ik_z \mathcal{H}_{\eta\eta} U' \mathcal{H}_{vv}. \quad (4)$$

The parameterization of \mathcal{H} is performed with respect to the streamwise/spanwise wavenumber and temporal frequency triplet, $\mathbf{k} = (k_x, k_z, \omega)$.

Apparently, \mathcal{H}_{vv} and $\mathcal{H}_{\eta v}$ are forced by \hat{g}_v only, while $\mathcal{H}_{\eta\eta}$ is forced by \hat{g}_η only. This motivates the separation of the response $\mathcal{H}\mathbf{p}$ into two distinct families:

$$\begin{pmatrix} \hat{v} \\ \hat{\eta}^{\text{OS}} \end{pmatrix} = \begin{pmatrix} \mathcal{H}_{vv} \\ \mathcal{H}_{\eta v} \end{pmatrix} \hat{g}_v, \quad (5)$$

$$\hat{\eta}^{\text{SQ}} = \mathcal{H}_{\eta\eta} \hat{g}_\eta. \quad (6)$$

In the following, we refer to the family of modes in Equation 5 as Orr-Sommerfeld (OS) modes and the family in Equation 6 as Squire (SQ) modes. The separation of $\hat{\eta}$ into two distinct families is common practice in linear stability analysis, where the SQ and OS modes are, respectively, the homogeneous and particular solutions of the Squire equation: $(-i\omega - \mathcal{L}^{\text{SQ}})\hat{\eta} = -ik_z U' \hat{v}$ [2]. That is, the OS modes can be interpreted as a response to the wall-normal velocity. This interpretation still holds in the nonlinear setting, since the second component of 5 can be written as $\hat{\eta}^{\text{OS}} = -ik_z \mathcal{H}_{\eta\eta} U' \hat{v}$. However, the SQ modes are no longer the homogeneous solutions, but are now interpreted as the response to forcing by \hat{g}_η .

Note that only the OS modes contain a \hat{v} response, such that the SQ modes contribute only to the $\hat{\eta}$ response, i.e., to the wall-parallel velocity components. There is thus the potential for interaction between the OS and SQ vorticity in ways that are not admitted by the standard resolvent decomposition. This fact is of central importance for the OS-SQ resolvent decomposition, and it will be demonstrated in what follows that this drastically improves the accuracy of a low-order resolvent-based representation of the second-order statistics for turbulent channel flow.

An SVD of each operator in Equation 5 is performed separately, and the resulting decomposition is referred to as the OS-SQ decomposition of the resolvent. The approximation of the response becomes

$$\begin{pmatrix} \hat{v} \\ \hat{\eta} \end{pmatrix} \approx \sum_{j=1}^{N^{\text{OS}}} \psi_j^{\text{OS}} \sigma_j^{\text{OS}} \chi_j^{\text{OS}} + \sum_{k=1}^{N^{\text{SQ}}} \psi_k^{\text{SQ}} \sigma_k^{\text{SQ}} \chi_k^{\text{SQ}}. \quad (7)$$

Note that Equation 7 is now a sum of $N^{\text{OS}} + N^{\text{SQ}}$ terms. Furthermore, while the left and right singular vectors of each family still comprise orthonormal sets with respect to the appropriate inner product, it is not guaranteed that modes belonging to different families are orthonormal, e.g. $\langle \psi_j^{\text{OS}}, \psi_k^{\text{SQ}} \rangle \neq \delta_{jk}$ in general.

3.1.2 Low-rank capture of linear response and nonlinear forcing in Exact Coherent States (ECS)

Rosenberg, K. & McKeon, B. J. Efficient representations of exact coherent states of the Navier-Stokes equations using resolvent analysis Fluid Dyn. Res., 51, 011401 (2019).

The decomposition above was applied to traveling wave ECS by [8], who showed that the method led to a low-order representation of both upper (not shown) and lower branch (Figure 2) solutions in terms of resolvent modes. In contrast to projection onto modes obtained from the full resolvent decomposition, all components of the Reynolds stresses were equally well-captured. Further, the nonlinear forcing (i.e., the gradients of Reynolds stress) was also captured in a low order way, meaning that this approach has the potential to capture both the linear and nonlinear components of Figure 1.

An iterative method to optimize mode weights by including both nonlinear interactions between scales, a constraint that the assumed mean profile was recovered and the requirement for a self-sustaining solution was also developed for ECS based on the Matlab function *fminunc* [9]. It was shown to converge to the true solution for equilibrium ECS (for the EQ1 solution in only 16 iterations), and remains under development as a promising tool to obtain nonlinear, self-sustaining solutions using the resolvent basis.

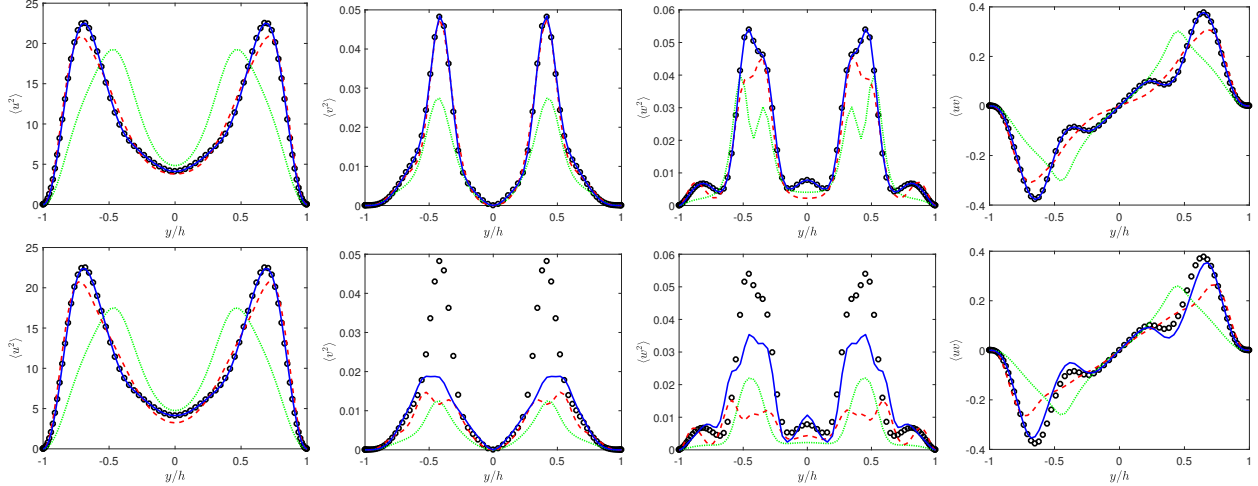


Figure 2: Comparison of the capture of the P4L traveling wave solution by the OS-SQ approach (top line) and the standard resolvent basis. Left to right: $\langle u^2 \rangle$, $\langle v^2 \rangle$, $\langle w^2 \rangle$, $\langle uv \rangle$. P4L solution (open circles), reconstruction with 1 (dotted green), 3 (dashed red), and 10 (solid blue) singular mode pairs.

3.1.3 Convergence to exact coherent solutions starting from the laminar velocity profile

Rosenberg, K. & McKeon, B. J. Computing exact coherent states in channels starting from the laminar profile: a resolvent-based approach *Phys. Rev. E* 100(2), 021101(2019).

A priori knowledge of $\mathbf{U}(y, z)$ can be considered a very limiting assumption. It has been demonstrated in [10] that progress can be made in finding ECS in Couette and Poiseuille flow starting from an initial laminar profile, based on an iterative procedure and resolvent analysis. We use the laminar profile as an input to the resolvent operator. The fluctuating velocity field is approximated by the leading singular mode of the resolvent operator. The nonlinear self-interaction is computed and used as the forcing into the mean momentum equation, which is solved to provide an updated mean velocity input. The procedure is then repeated until three conditions are met: (i) the cycle self-sustains (i.e. the updated mean profile, $\mathbf{U}(y, z)$, converges), (ii) the resolvent associated with the new mean velocity is itself low-rank, and (iii) $\mathbf{U}(y, z)$ is (nearly) neutrally stable.

Figure 3 shows the results for Poiseuille flow: the magnitude of the \hat{u} , \hat{v} , and \hat{w} components of the fundamental streamwise Fourier mode, along with the resulting mean velocity field (deviation from laminar). The first three columns show the first, second, and fifth iterations respectively and the last column showing the converged solution obtained from Channelflow (requiring four Newton iterations). There is a close correspondence between the final iteration and the true solution (relative error of 1.4%), as well as localization of the fluctuations around the critical layer $U(y, z) = c = 0.88$. This ECS solution has not been previously reported, to our knowledge.

The approach represents a low-order, resolvent-based method to compute self-sustaining solutions for lower branch ECS in channels, requiring the specification of only two unknown parameters, namely the wavespeed and amplitude of a single streamwise-varying Fourier mode. The low-dimensionality of the approach leverages the properties of the resolvent operator for the underlying (nearly) neutrally stable (streamwise-averaged) mean flow and perhaps suggests that (lower-branch) solutions of the Navier-Stokes equation can be described in extraordinarily simple forms.

The framework is quite general in its formulation and could be applied to other exact solutions. In addition to starting from a laminar solution, simple analytic expressions for the mean forcing may be useful to generate an initial roll/streak mean flow, as explored by [11] and [12]. A potential improvement to the current formulation would be to incorporate an optimization step to more directly drive the mean flow towards a neutrally stable configuration. While the current approach seems only applicable to lower-branch states at

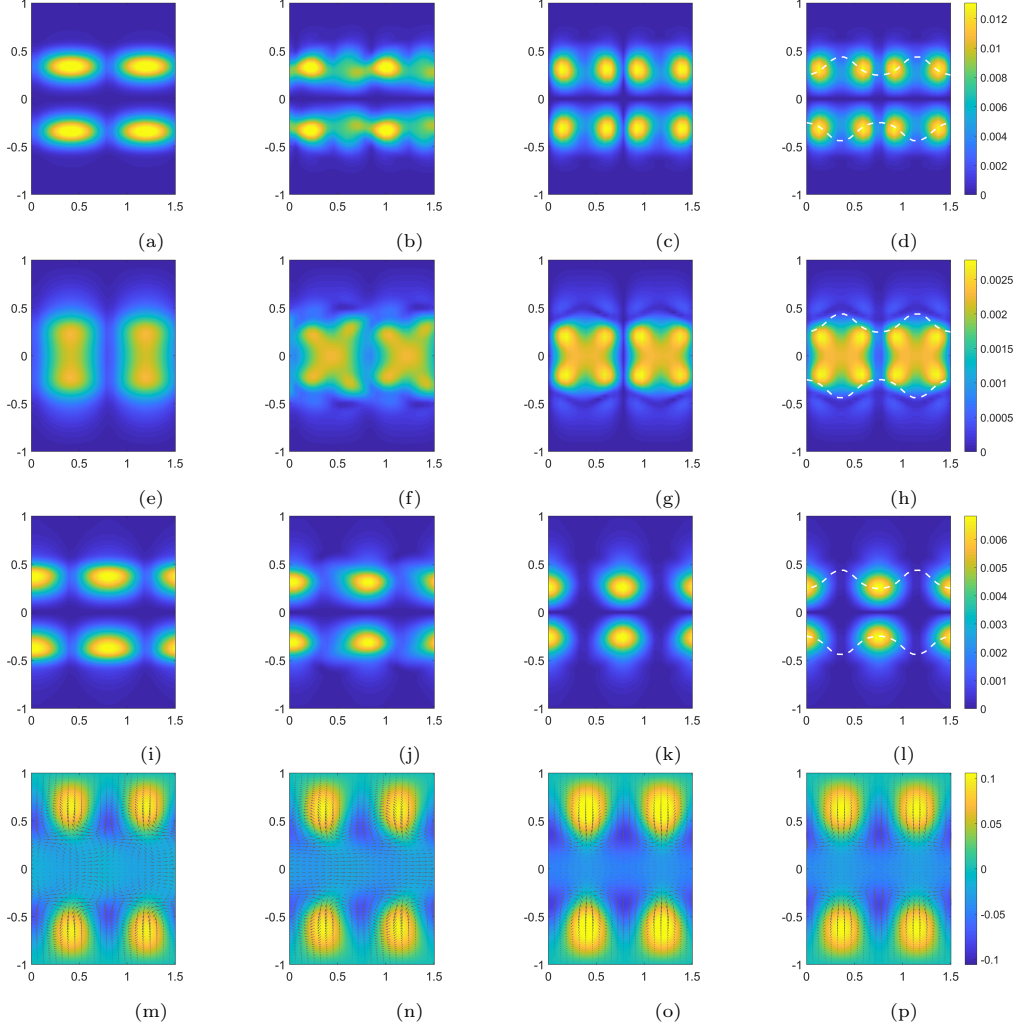


Figure 3: Poiseuille flow: The amplitude as a function of spanwise (horizontal axis) and wall-normal (vertical axis) distance of the (a)-(d) u-component, (e)-(h) v-component, and (i)-(l) w-component of the fundamental streamwise Fourier mode k_{x_f} along with the (m)-(p) resulting mean velocity $\mathbf{U}(y, z)$ (shown as the deviation from laminar) generated from the self-interaction of the single Fourier mode. The first three columns represent the first, second, and fifth iterations respectively for an initial laminar profile, and the last column shows the converged field computed using Channelflow with iteration 5 as an input. The white dashed line in the last column designates the location of the critical layer, $U(y, z) = c = 0.88$.

these moderate Reynolds numbers, there is evidence these ideas can be extended to upper-branch states, though at higher Reynolds numbers [13], and is a subject of future work; however, flows with more than one energetically significant streamwise-varying mode would require more sophisticated modeling efforts. We wish to eventually extend this methodology to the computation of periodic orbits as well. Ultimately, we hope the results presented herein will inform the continued efforts to model turbulence using the 2D/3C framework, particularly by augmenting them with frequency-based input/output (resolvent-based) techniques.

3.1.4 Optimization of resolvent mode weights in fully-turbulent channel flow

McMullen, R., Rosenberg, K. & McKeon, B. J. Interaction of Orr-Sommerfeld and Squire modes in a low-order model of turbulent channel flow (In preparation.)

While the utility of the decomposition into Orr-Sommerfeld and Squire modes for highly simplified flows like ECS has been established, an open question is whether or not it remains relevant for high Reynolds number turbulence. In this work, it has been shown that the second-order statistics of turbulent channel flow can be accurately modeled using a low-order approximation based on this framework. It was additionally shown that the vorticity produced by the Orr-Sommerfeld and Squire modes act to oppose each other, and this observation reveals information about how the resolvent weights for the two families scale relative to each other with Reynolds number. Altogether, these insights point to a mechanism in wall-bounded turbulent flows (here channel flow) that is important for low-order modeling efforts.

As introduced by [6], the model three-dimensional streamwise energy spectra are

$$E_r(y, k_x, k_z, c) = \text{Re}\{\text{tr}(\mathbf{A}_r \mathbf{X})\}, \quad (8)$$

with $r \in \{uu, vv, ww, uv\}$, and where $\text{Re}\{\cdot\}$ is the real part of a complex number and $\text{tr}(\cdot)$ is the matrix trace. Note that we have chosen to parameterize the spectra in terms of the wavespeed $c = \omega/k_x$ since resolvent modes tend to be localized about the critical layers y_c , where $U(y_c) = c$ [1], and it has been observed experimentally that the range of energetic wavespeeds is relatively compact, with the most energetic motions typically being confined to the range $8 \lesssim c \lesssim U_{cl}$ [14], where U_{cl} is the mean centerline velocity. In Equation 8, the matrix \mathbf{A}_{uu} , for example, with entries

$$\mathbf{A}_{uu,ij} = \sigma_i \sigma_j \hat{u}_i \hat{u}_j^*, \quad (9)$$

represents the contributions of the singular values and response modes and can be determined *a priori* from the SVD of the resolvent. The matrix \mathbf{X} , with entries

$$\mathbf{X}_{ij} = \chi_i^* \chi_j, \quad (10)$$

is the weights matrix. Apparent from this definition is that $\mathbf{X}^T = \chi \chi^* \geq \mathbf{0}$, where χ is the vector of weights and \geq denotes the Löwner order, i.e., \mathbf{X} is a rank-1 positive-semidefinite matrix. The OS-SQ decomposition is incorporated into this framework simply by partitioning the \mathbf{A}_r and \mathbf{X} matrices as

$$\mathbf{A}_r = \begin{pmatrix} \mathbf{A}_r^{\text{OS/OS}} & \mathbf{A}_r^{\text{OS/SQ}} \\ \mathbf{A}_r^{\text{SQ/OS}} & \mathbf{A}_r^{\text{SQ/SQ}} \end{pmatrix}, \quad \mathbf{X} = \begin{pmatrix} \mathbf{X}^{\text{OS/OS}} & \mathbf{X}^{\text{OS/SQ}} \\ \mathbf{X}^{\text{OS/SQ}*} & \mathbf{X}^{\text{SQ/SQ}} \end{pmatrix}, \quad (11)$$

where the superscript X/Y denotes the family of the i th and j th mode, respectively, in Equations 9-10.

The goal is to compute the weights matrix such that the deviation between the wavespeed-integrated model spectra in 8 and the time-averaged DNS spectra is minimized. After discretization of the wavespeed range $c \in [0, U_{cl}]$, this can be formally cast as the following optimization problem: For fixed k_x and k_z ,

$$\begin{aligned} & \underset{\{\mathbf{X}_l\}_{l=1,2,\dots,N_c}, e}{\text{minimize}} && e \\ & \text{subject to} && \frac{\|E_r^{\text{DNS}} - \sum_{l=1}^{N_c} k_x \text{dc Re}\{\text{tr}(\mathbf{A}_{r,l} \mathbf{X}_l)\}\|^2}{\|E_r^{\text{DNS}}\|^2} \leq e \\ & && \mathbf{X}_l \geq \mathbf{0}, l = 1, 2, \dots, N_c, \end{aligned} \quad (12)$$

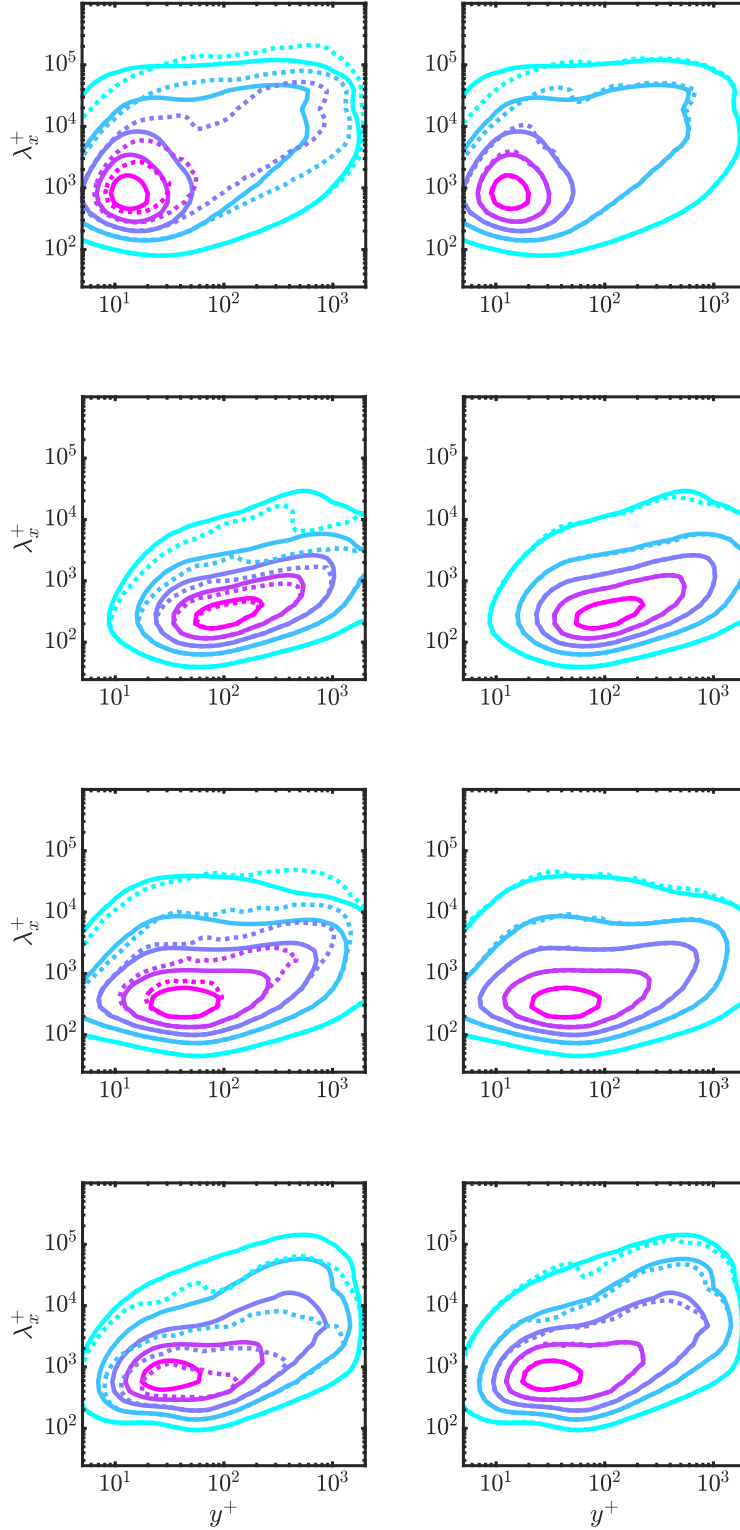


Figure 4: Premultiplied one-dimensional spectra from the model (dotted contours) and DNS (solid contours). (a,c,e,g) Standard resolvent decomposition using $N = 6$ modes per wavenumber-frequency triplet; (b,d,f,h) OS-SQ resolvent decomposition using $N^{\text{OS}} = N^{\text{SQ}} = 3$ modes per wavenumber-frequency triplet. (a,b) $k_x E_{uu}$, (c,d) $k_x E_{vv}$, (e,f) $k_x E_{wv}$, (g,h) $-k_x E_{uv}$. Contour levels are from 10% to 90% of the DNS maximum in 20% increments.

where the subscript l denotes a quantity evaluated at $c = c_l$. Note that the norm $\|\cdot\|$ is not the simple kinetic energy norm. It is defined as

$$\|f\|^2 = \int_{y_{\min}^+}^{y_{\max}^+} |f(\log y^+)|^2 d \log y^+ \quad (13)$$

and is designed to penalize deviations across the channel equally [6]. Thus deviations from the DNS spectra are enforced for $y_{\min}^+ \leq y^+ \leq y_{\max}^+$, where we take $y_{\min}^+ = 5$ and $y_{\max}^+ = Re_\tau - 1$.

Equations 12 represent a semidefinite program (SDP) for the weights matrices \mathbf{X}_l and can therefore be solved efficiently using a convex optimization software package. Note that imposing the rank-1 constraint on the \mathbf{X}_l would make 12 non-convex. [6] employed an iterative rank-reduction procedure to recover rank-1 matrices from the full-rank solution [15]. However, we do not employ this algorithm here and instead choose to work with the full-rank weights matrices. In this case, the \mathbf{X}_l can be interpreted as the covariance matrices of the weights, similar to [16]. Finally, since the optimization is performed for second-order statistics, the present approach does not provide phase information about modes with different wavenumbers. This means that the computed weights do not yield a closed, self-consistent system, as such information is necessary to recover the mean velocity profile. Extension of the method to incorporate phase is a direction for future work.

The performance of the model spectra obtained by integrating over all resolvent modes is evaluated by comparing them to the time-averaged statistics from the DNS. The premultiplied 1D k_x model spectra,

$$k_x E_\tau(y, k_x) = \int_{k_z, \min}^{k_z, \max} \int_0^{U_{cl}} k_x^2 E_\tau(y, k_x, k_z, c) dc dk_z, \quad (14)$$

are compared to the DNS using $N^{OS} = N^{SQ} = 3$ modes, i.e., six modes per wavenumber-frequency triplet, in Figure 4, which is plotted in terms of $\lambda_x^+ = 2\pi/k_x^+$. Overall, the agreement between the model and DNS spectra is very good, and in particular, the peaks are captured well. Also shown are the spectra obtained using the standard decomposition with the same total number of modes. The performance is significantly worse, with $k_x E_{uu}$ and $k_x E_{ww}$ being greatly over-predicted, and $k_x E_{vv}$ and $-k_x E_{uv}$ being under-predicted.

Subsequent integration over k_x gives the intensities, which are shown in figure 5. The deviation errors are 4.3%, 0.95%, 0.66%, and 3.8% for $\langle u^2 \rangle$, $\langle v^2 \rangle$, $\langle w^2 \rangle$, and $\langle -uv \rangle$, respectively. These should be compared with errors of 30%, 14%, 12%, and 31% using the standard resolvent decomposition, shown in the dashed curves. The OS/SQ basis gives very good agreement with the data with a significant reduction in degrees of freedom: only six modes per wavenumber-frequency triplet.

To further examine the relationship between the OS and SQ modes, we decompose the intensities shown in 5 into contributions from OS modes only, SQ modes only, and a cross term (C) that represents the interaction of OS and SQ modes, e.g. $\langle u^2 \rangle$ becomes

$$\langle u^2 \rangle = \underbrace{\langle (u^{OS})^2 \rangle}_{OS} + \underbrace{\langle (u^{SQ})^2 \rangle}_{SQ} + 2 \underbrace{\langle u^{OS} u^{SQ} \rangle}_C. \quad (15)$$

The results with $N = 3$ for $\langle u^2 \rangle$, $\langle w^2 \rangle$, and $\langle -uv \rangle$ are shown in 6. The decomposition for $\langle v^2 \rangle$ is not shown since, as seen from 6, the SQ modes have no v response, and hence $\langle v^2 \rangle = \langle (v^{OS})^2 \rangle$. Similarly, there is no SQ-only contribution to $\langle -uv \rangle$. For $\langle u^2 \rangle$ and $\langle w^2 \rangle$, the OS and SQ terms are extremely similar, with the OS term having slightly larger magnitude. However, for all three components the C term is negative, which supports the claim that the SQ vorticity acts to saturate the OS vorticity. In fact, information about the phase relationship between the OS and SQ modes can be deduced from this observation. Note that the third term in 15 is simply twice the covariance of u^{OS} and u^{SQ} .

In summary, the OS/SQ decomposition that we previously applied to the ECS solution is shown to be important for efficient representation of fully turbulent velocity fields from DNS, with the same opposing phase relationship leading to saturation of the wall-normal vorticity relative to the standard resolvent decomposition.

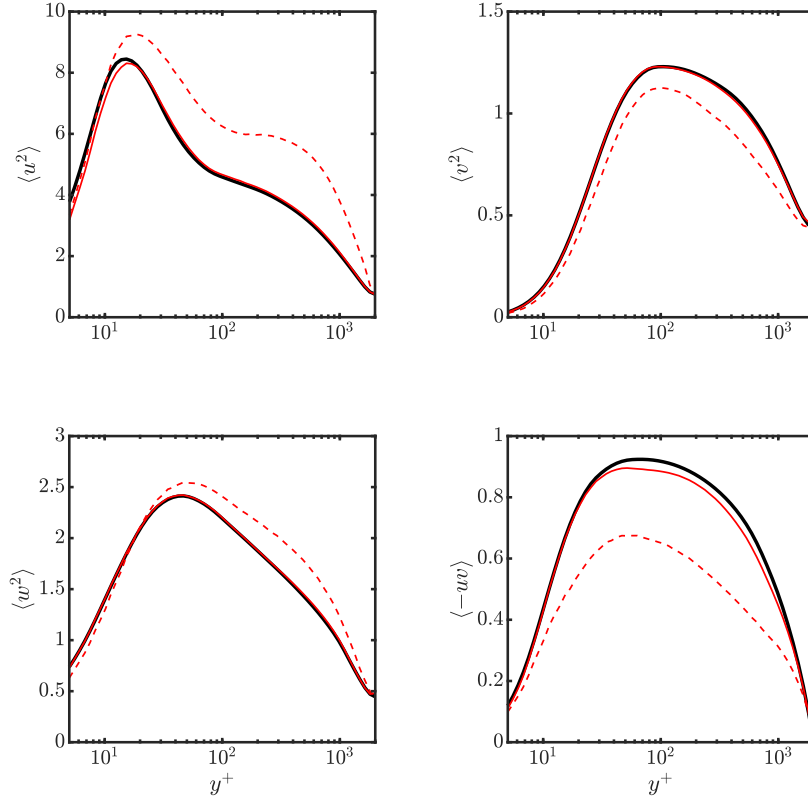


Figure 5: Intensities from the model with $N^{\text{OS}} = N^{\text{SQ}} = 3$ modes per wavenumber-frequency triplet (—) and DNS (—). Also shown in dashed lines are the intensities obtained from the standard resolvent decomposition approach using the same total number of modes.

3.1.5 Scaling of resolvent mode weights by consideration of mode interactions

McMullen, R., Rosenberg, K. & McKeon, B. J. Interaction of Orr-Sommerfeld and Squire modes in a low-order model of turbulent channel flow (In preparation.)

Further progress in determining Reynolds number scaling can be made using the mode weights (strictly the mode magnitudes) determined from the optimization above and the properties of the mean velocity profile. Moarref et al. [3] leveraged universal scaling regimes of the mean velocity profile to derive the Re scaling for several universal classes of resolvent modes. Here, we extend this to the OS-SQ resolvent decomposition, showing analytically and with reference to the optimized weights that for the outer and geometrically self-similar classes, each family of modes has a distinct scaling for the singular values. From this, the scalings of each submatrix of the energy density matrices \mathbf{A}_r given in Equation 11 can be determined. Combining these scalings with the hypothesis that competition of the OS and SQ modes remains relevant at different Reynolds numbers and in different regions of the flow enables the relative scaling of the OS and SQ weights belonging to the universal classes to be deduced.

The universal classes investigated here are the inner, outer, and geometrically self-similar classes. These consist of resolvent modes that are localized within the near-wall, wake, and logarithmic regions of the flow, respectively, and rely on universality of the mean velocity profile under the appropriate scaling in these regions.

The outer class length scales are

$$\tilde{k}_x = Re k_x, \quad \tilde{k}_z = k_z, \quad \tilde{y} = y, \quad (16)$$

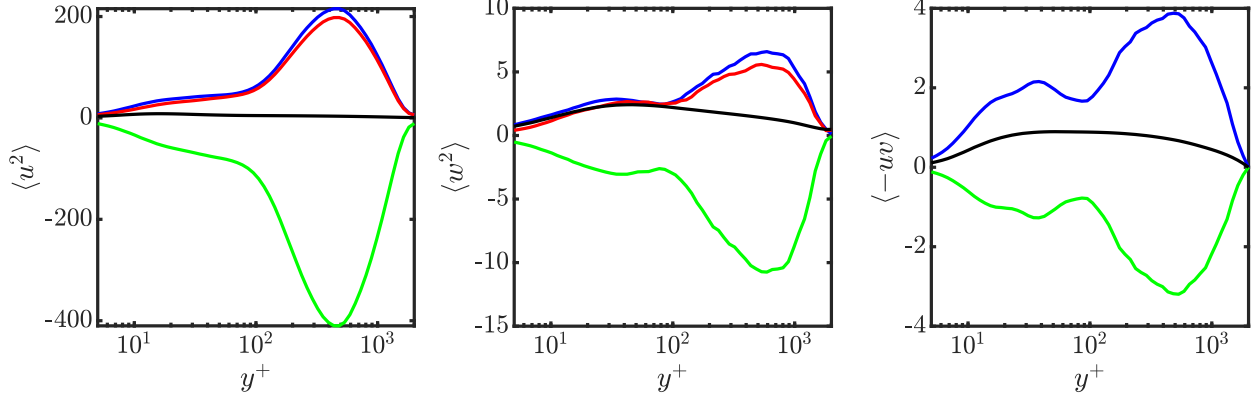


Figure 6: (a) $\langle u^2 \rangle$, (b) $\langle w^2 \rangle$, (c) $\langle -uw \rangle$ decomposed into OS (—), SQ (—), and C (—) terms for $N = 3$.

and the outer class wave parameters are

$$\mathcal{S}_o : \begin{cases} 0 \leq U_{cl} - c \lesssim 6.17 \\ k_z/k_x \gtrsim \gamma Re/Re_{\tau, \min} \end{cases} \quad (17)$$

The upper bound on the wavespeed defect $U_{cl} - c = 6.17$ is obtained from the setting the minimum critical layer location at the bottom of the outer region, i.e., $U_{cl} - U(y = 0.1) = 6.17$. As Equation 17 indicates, the outer class modes must satisfy an aspect ratio constraint for all Re considered, where the minimum aspect ratio is γ when $Re = Re_{\tau, \min}$ [3]. Here, $Re_{\tau, \min} = 934$. From Equation 16 and continuity, it follows that

$$\hat{\mathbf{u}} = \begin{pmatrix} \tilde{u} \\ Re^{-1} \tilde{v} \\ Re^{-1} \tilde{w} \end{pmatrix}. \quad (18)$$

where $\tilde{\cdot}$ indicates a quantity that is approximately Re -invariant for modes belonging to the outer class. See also [17] and [18] for the scaling of each velocity component, as well as for the components of the forcing modes.

The outer-scaled versions of the weighted resolvent operators are

$$\begin{pmatrix} \mathbf{F}_v \mathcal{H}_{vv} \mathbf{F}_v^{-1} \\ \mathbf{F}_\eta \mathcal{H}_{\eta v} \mathbf{F}_v^{-1} \end{pmatrix} = \begin{pmatrix} Re \tilde{\mathbf{F}}_v \tilde{\mathcal{H}}_{vv} \tilde{\mathbf{F}}_v^{-1} \\ Re^2 \tilde{\mathbf{F}}_\eta \tilde{\mathcal{H}}_{\eta v} \tilde{\mathbf{F}}_v^{-1} \end{pmatrix} \quad (19)$$

$$\mathbf{F}_\eta \mathcal{H}_{\eta\eta} \mathbf{F}_\eta^{-1} = Re \tilde{\mathbf{F}}_\eta \tilde{\mathcal{H}}_{\eta\eta} \tilde{\mathbf{F}}_\eta^{-1}. \quad (20)$$

Performing the SVDs of Equations 19 and 20, we have for the leading singular values,

$$\sigma_j^{\text{OS}} = Re^2 \tilde{\sigma}_j^{\text{OS}}, \quad \sigma_j^{\text{SQ}} = Re \tilde{\sigma}_j^{\text{SQ}}. \quad (21)$$

Note that because the components of 19 do not scale uniformly for outer class modes, the scaling of the OS singular values is only expected to hold for the first several modes. However, since good agreement between the model and DNS spectra is achieved using only a small number of modes, it is reasonable to adopt the scalings in what follows.

As for the inner class modes, competition between the OS and SQ modes requires that all three terms are of the same order for arbitrary Re , which is satisfied if

$$\left| \frac{\chi_j^{\text{SQ}}}{\chi_j^{\text{OS}}} \right| \sim Re \quad (22)$$

for modes belonging to the universal outer class.

The weights ratio $\sqrt{X_{11}^{\text{SQ/SQ}}/X_{11}^{\text{OS/OS}}}$ for the three Reynolds numbers is shown in the top row of 7 for several values of the outer-scaled wavenumber combinations $(\tilde{k}_x, \tilde{k}_x)$ and a minimum aspect ratio $\gamma = \sqrt{10}$. In agreement with 22, the data from all three Reynolds numbers show reasonable collapse onto a single curve for $U_{cl} - c \lesssim 6.17$ when scaled by Re^{-1} , as seen in the bottom row of 7.

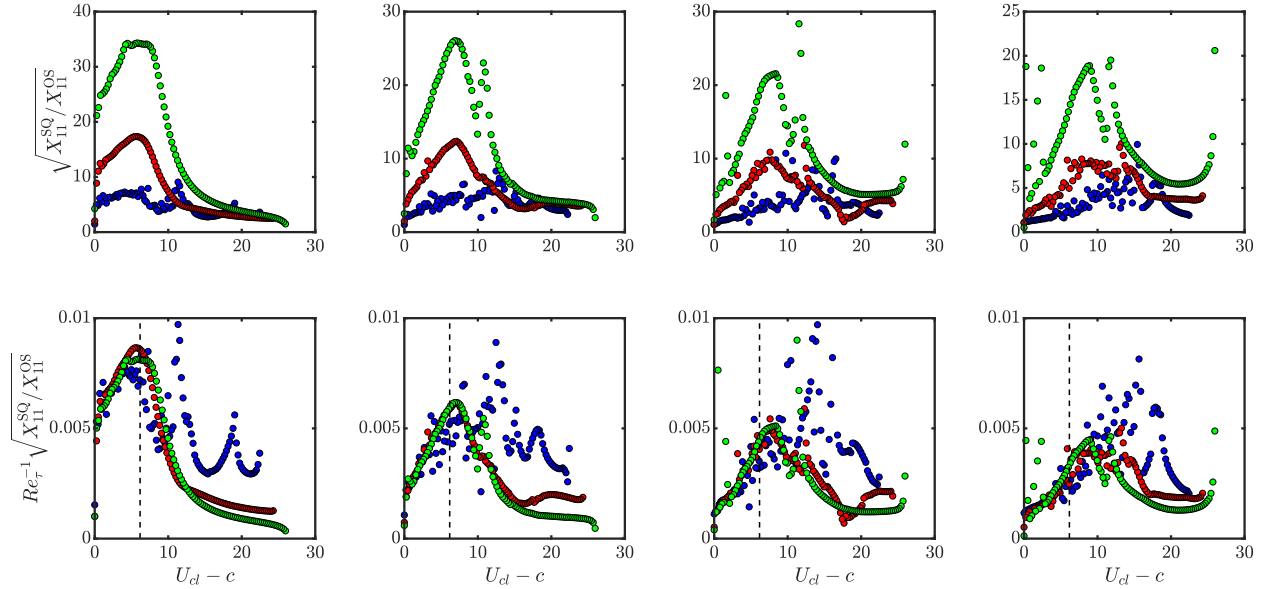


Figure 7: (a)-(d) Leading weights ratio for $Re = 934$ (blue), $Re = 2003$ (red), and $Re = 4219$ (green) with $N = 2$. (e)-(h) Weights ratio scaled according to 22. Each column represents a different scaled streamwise wavenumber \tilde{k}_x : (a),(e) $\tilde{k}_x = 4219$; (b),(f) $\tilde{k}_x = 8438$; (c),(g) $\tilde{k}_x = 12657$; (d),(h) $\tilde{k}_x = 16876$. In all cases the spanwise wavenumber is $\tilde{k}_z = \gamma \tilde{k}_x / Re_{\tau, \min}$, with $\gamma = \sqrt{10}$. The dashed line indicates the upper end of the wavespeed defect range, $U_{cl} - c = 6.17$, where the outer class scaling is expected to hold.

Related results can be obtained by consideration of the inner and logarithmic scaling regions of the mean velocity profile, where the former has special implications for self-similarity and self-sustaining turbulence, e.g. [19].

Some preliminary steps have been made towards reconciliation of resolvent analysis and results from the mean momentum balance approach, but further advances will require additional progress with regards to the mode weights, as under investigation [20].

3.2 Experimental excitation of a triadic interaction

McKeon, B. J., Jacobi, I. & Duvvuri, S. Dynamic roughness for manipulation and control of turbulent boundary layers: a review. AIAA J., 56(6) 2179-2193 (2018).

This grant funded an experimental study on the generation and characterization of synthetic triadic interactions in a turbulent boundary layer using dynamic roughness actuation (Figure 8). Preliminary work is reported in [21], then expanded and discussed in [22].

These measurements, reported in [23], show for the first time clear evidence of the direct triadic interaction of large-scale velocity modes in the turbulent boundary layer. This had been hinted at in the single frequency experiments by the excitation of harmonics and via the integrated observations of the preceding section, but the triadic nature of the coupling was not directly observable from within the shroud of the envelope of the small scale motions.

The harmonic excitation of two frequencies using a dynamic roughness forcing (a spanwise rib, oscillating from flush with the plate to a constant amplitude with harmonic waveform) permits reconstruction of the

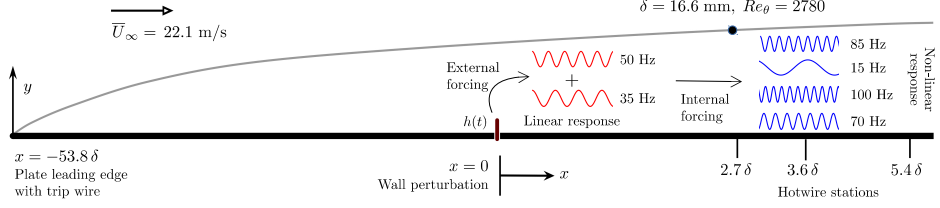


Figure 8: Schematic of the directly excited nonlinear interactions, from [23]

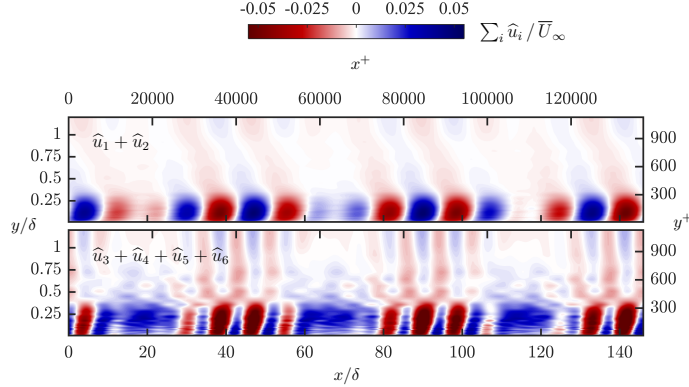


Figure 9: Synthetic turbulence fields. Top: linearly excited modes, $\hat{\mathbf{u}}_1 + \hat{\mathbf{u}}_2$ (from Duvvuri & McKeon [21]). Bottom: sum of directly excited modes, $\hat{\mathbf{u}}_3 + \hat{\mathbf{u}}_4 + \hat{\mathbf{u}}_5 + \hat{\mathbf{u}}_6$.

boundary layer response associated with the two forced modes as well as four triadically coupled modes excited by direct nonlinear interaction (sum, difference and two harmonics at twice the forcing frequencies). Temporal phase variations, $\phi(t)$, can be converted to the spatial domain, a process which is simplified because all modes have the same convection velocity. Figure 9 shows the linearly excited field, i.e. $\hat{\mathbf{u}}_1 + \hat{\mathbf{u}}_2$, and the directly excited, synthetic turbulence field, $\hat{\mathbf{u}}_3 + \hat{\mathbf{u}}_4 + \hat{\mathbf{u}}_5 + \hat{\mathbf{u}}_6$.

The success of this simple study in a turbulent boundary layer - which the Navier-Stokes equations dictate! - suggests the ability to excite scales indirectly within the boundary layer by means of the non-linear coupling between the desired scales and the forced scales, and further to create and characterize a synthetic contribution to a turbulent boundary layer.

3.3 New approaches to turbulence modeling and control

3.3.1 Measures of non-normality

Symon, S., Rosenberg, K., Dawson, S. T. M. & McKeon, B. J. Non-normality and classification of amplification mechanisms associated with turbulent mean flows Phys. Rev. Fluids, 3(5), 053902 (2018)

We investigated the nature of the non-normality of the resolvent and compared it to results from stability, i.e. the eigenspectrum of the NSE linearized about the laminar base flow, in order to gain further understanding concerning the origin of amplification in resolvent analysis. Eigenspectra and pseudospectra of the mean-linearized Navier-Stokes operator were used to characterize amplification mechanisms in laminar and turbulent flows in which linear mechanisms are important. Success of mean flow (linear) stability analysis for a particular frequency was shown to depend on whether two scalar measures of non-normality agree: (1) the product between the resolvent norm and the distance from the imaginary axis to the closest eigenvalue and (2) the inverse of the inner product between the most amplified resolvent forcing and response modes. If they agree, the resolvent operator can be rewritten in its dyadic representation to reveal that adjoint and forward stability modes are proportional to forcing and response resolvent modes at that frequency. Hence the real

parts of the eigenvalues are important since they are responsible for resonant amplification and the resolvent operator is low rank when the eigenvalues are sufficiently separated in the spectrum. If the amplification is pseudoresonant, then resolvent analysis is more suitable to understand the origin of flow structures.

Two test cases were studied: low Reynolds number cylinder flow and turbulent channel flow. The first deals mainly with resonant mechanisms, hence the success of both classical and mean stability analysis with respect to predicting the critical Reynolds number and global frequency of the saturated flow. Both scalar measures of non-normality agree for the base and mean flows, and the region where the forcing and response modes overlap scales with the length of the recirculation bubble. In the case of turbulent channel flow, structures result from both resonant and pseudoresonant mechanisms, suggesting that both are necessary elements to sustain turbulence. Mean shear is exploited most efficiently by stationary disturbances while bounds on the pseudospectra illustrate how pseudoresonance is responsible for the most amplified disturbances at spatial wavenumbers and temporal frequencies corresponding to well-known turbulent structures.

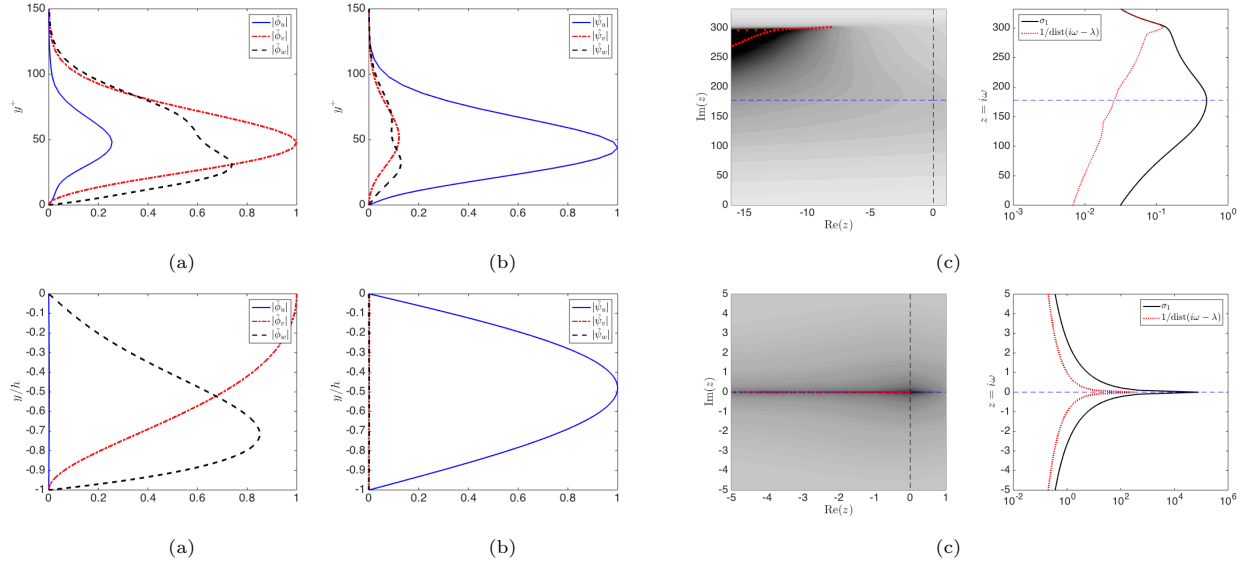


Figure 10: Spectral results for (top) a mode representative of the near-wall cycle and (bottom) corresponding to the wavenumber triplet of $(k_x, k_z, \omega) = (0, 2\pi/3, 0)$. Left-to-right: velocity amplitudes for the optimal forcing mode, and the optimal response mode, the eigenvalues of the associated linearized NSE operator in red circles overlaid with contours of the pseudospectrum, and the resolvent norm (solid black line) along with the inverse distance from the imaginary axis to the nearest eigenvalue (dotted red line).

3.3.2 Coherent structures and uniform momentum zones from resolvent modes

Saxton-Fox, T. & McKeon, B. J. Coherent structures, uniform momentum zones and the streamwise energy spectrum in wall-bounded turbulent flows J. Fluid Mech., 826, R6, 1-12 (2017)

It has been shown [24] that coherent bulges in velocity isocontours and uniform momentum, commonly observed in experiment and simulation, have a simple representation via resolvent modes using the first singular vector at a wavenumber-frequency combination representative of large-scale motions (LSMs). Figure 11 shows the three-dimensional structure of the LSM representative model with and without the mean velocity field superimposed, and a comparison between the instantaneous flow field in a wall-normal-streamwise field from the simple model and PIV data for $Re_\tau = 900$. In (a), the streamwise velocity isosurface is seen to alternate between protruding above and protruding below its mean position, giving the appearance of bulges. In (b), the structure is observed to be periodic in the streamwise and spanwise directions, with a compact wall-normal coherence and a phase change of π across its height. The structure of the LSM representative model compares favourably with that of the instantaneous structure in the PIV data. In

the laboratory frame velocity field, a positive fluctuating structure corresponds to the absence of a visible structure (downward protrusion of isocontours), and the streamwise length scale of the structure, which is constant in the fluctuating field, is observed to change as a function of the wall-normal height. The amplitude of the LSM representative model was deduced from a single frame of PIV, and is therefore the largest source of uncertainty in the model.

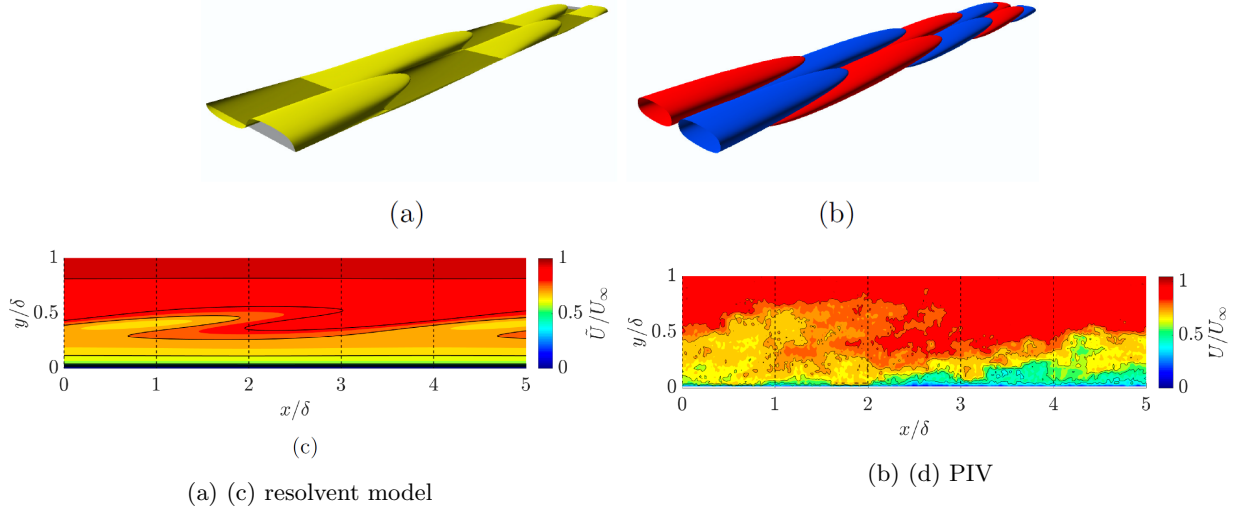


Figure 11: Instantaneous streamwise velocity field \tilde{U} (a) and fluctuating velocity field \tilde{u} (b) from an LSM-representative resolvent mode. In (c), a wall-normal-streamwise slice of the laboratory frame velocity field is shown with the contour range $\tilde{U}/U_\infty = 0 : 0.05 : 1$ and every other isocontour outlined in black for visibility. Representative snapshot from laboratory PIV with the same colorscale (d).

An analytical relationship between a laboratory frame streamwise velocity isocontour and the fluctuating velocity field was derived and used to generate model histograms of instantaneous velocity over various windows, with reasonable comparison to the results from PIV data (at a level perhaps surprising for such a simple model). A model of a single scale can reproduce two UMZs. Then it can be anticipated that the superposition of a very small number of such models could lead to the three to five UMZs observed across $Re_\tau = 10^3 - 10^4$ by [25]. Superposition of a few scales that are dominant in the energy spectrum, e.g. from the LSM energy band, the superstructures or VLSMs and the near-wall cycle, would lead to a modelled flow that is compatible with the energetic features of real wall-bounded flows. Superposition of multiple modes can also be used to allow for the representation of more complex phenomena, such as the meandering of structures [26] and amplitude modulation of small scales [5].

3.3.3 Resolvent as a tool to evaluate control technologies - Opposition control example

Toedtli, S., Luhar, M. & McKeon, B. J. Predicting the response of turbulent channel flow to varying-phase opposition control: Resolvent analysis as a tool for flow control design *Phys. Rev. Fluids*, 4(7), 073905 (2019)

We have evaluated the capabilities of a low-order flow model based on resolvent analysis for the purpose of controller design for drag reduction in wall-bounded turbulent flows. We modified the analysis to account for an opposition control boundary condition in earlier work [27]. Here we use Direct Numerical Simulation studies to show that the model is able to approximate the trends in mean wall shear stress, which is commonly used as measure for drag reduction. We also derive an analytical expression that decomposes the drag reduction in internal flows into terms that can be predicted directly by the model and terms that allow for quantification of model error if high-fidelity data are available. We then show by example of varying-phase opposition control in a low-Reynolds-number turbulent channel flow that the drag reduction predicted by the resolvent

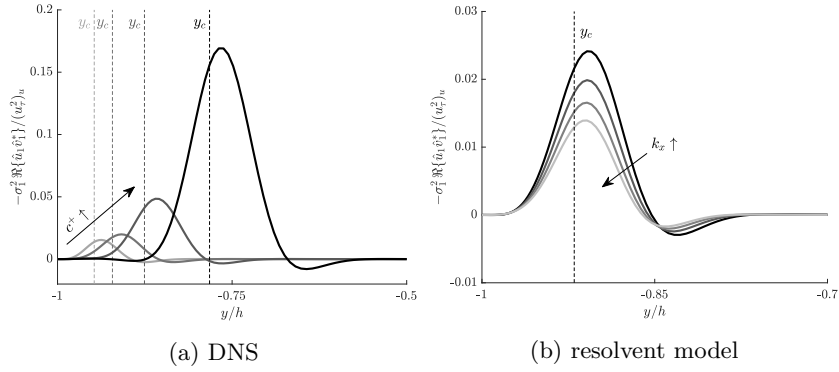


Figure 12: Effect of wave speed and streamwise wave number on the mean Reynolds stress contribution of individual resolvent modes: (a) effect of wave speed c (darker colors indicate faster wave speeds), and (b) effect of streamwise wave number k_x (darker colors indicating smaller streamwise wave numbers).

model captures the trend observed in direct numerical simulation (DNS) over a wide range of controller parameters. The DNS results confirm the resolvent model prediction that the attainable drag reduction strongly depends on the relative phase between sensor measurement and actuator response, which raises interesting flow physics questions for future studies. The good agreement between the resolvent model and DNS further reveals that resolvent analysis, which at its heart is a linear technique, is able to approximate the response of the full nonlinear system to control.

While performing this work, we also formalized a sub-sampling techniques that exploits the characteristics of the resolvent operator to further reduce the degrees of freedom required to model the flow under opposition control. We have previously shown, e.g. [27], that the Reynolds stress contribution of a single mode is localized around its critical layer, i.e. around the wall-normal location y_c where its wavespeed equals the local mean velocity $c \approx \bar{u}(y_c)$. Conversely, one can say that the dominant contribution to the Reynolds stress at a fixed y comes from modes whose critical layer y_c correspond to that y . From the previous argument we expect that the dominant Reynolds stress contribution at each gridpoint y_i is given by modes with wavespeed $c = \bar{u}(y_i)$. This suggests that the sampled wavespeeds should correspond to the discretized mean velocity profile, so that $0 \leq \omega \leq k_x U_{cl}$ (as mentioned before) and $\Delta\omega_i(k_x) = k_x \Delta\bar{u}(y_i)$. Note that while empirical knowledge is required to justify this range of ω , no empirical knowledge is required to evaluate it: the temporal frequency vector is fully determined by the given mean velocity profile and wall-normal grid. The localization of the mean Reynolds stress contribution of individual modes around the critical layer, y_c , is shown in Figures 12a and 12b for varying c and k_x , respectively. The wall-normal profiles for different c look very similar and the location of their peak moves slowly away from the wall as the wave speed is increased. This suggests that not all the wave speeds resolved in the model baseline are required to capture the wall-normal shape of the mean Reynolds stress profile, since resolvent modes with similar wave speeds largely overlap in y . The wall-normal profiles look very similar for various k_x and that the peak magnitude slowly decreases as k_x increases. This observation holds for all sufficiently large streamwise and spanwise wave numbers and suggests that the spatial wave numbers can be subsampled as well as the wave speeds.

Based on these insights, a sub-sampling was employed in the control studies corresponding to a reduction in degrees of freedom from $85 \times 85 \times 86$ (baseline) to $16 \times 22 \times 44$ (subsamped model) resolved wave numbers. The missing wave numbers are linearly interpolated. The resolvent model for the Reynolds stress was calculated by assessing the $-uv$ contributed by the summation of first resolvent modes across wavenumbers and frequencies, weighted by their singular values, i.e. the response to unit amplitude broadband forcing. A comparison of the Reynolds stress arising from the full and sub-sampled resolvent models for uncontrolled channel flow is shown in Figure 13b. The agreement is excellent, thus, in order to make accurate predictions the model only needs to resolve a small subset of the DNS wave numbers. Further (not shown), the controlled resolvent modes obey the Reynolds number scaling laws of the uncontrolled resolvent operator derived by [3].

The varying-phase opposition control scheme (9) introduced in the preceding section is used as a test to

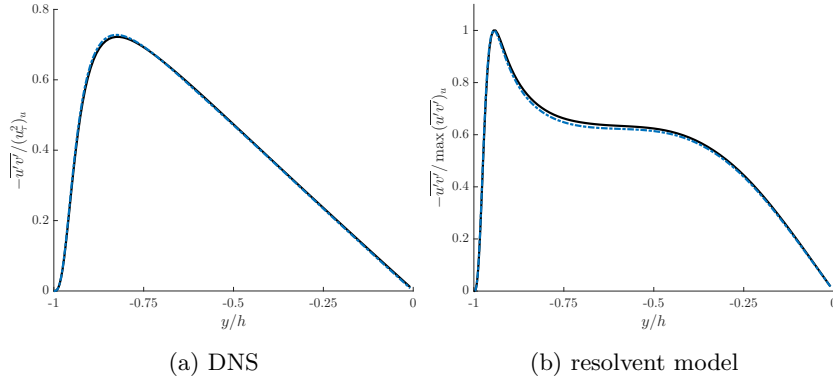


Figure 13: Uncontrolled Reynolds stress profiles from DNS and the resolvent model. Figure (a): (blue) DNS data of Lee & Moser [28] (uncontrolled flow), (black) present DNS (uncontrolled flow). Figure (b): (blue) resolvent model baseline (uncontrolled flow), (black) subsampled model (uncontrolled flow). Note that the resolvent model predictions are normalized with the maximum Reynolds stress of the uncontrolled profile.

evaluate the capabilities of the resolvent model for controller design. To this end, a total of 50 simulations of opposition control were performed, covering a parameter range of five sensor locations $y_d^+ = [5, 10, 15, 20, 25]$ and ten phase shifts between the sensed wall normal velocity and the (negative of) the wall transpiration (actuation) in response, $\angle A_d = [3\pi/4, \pi/2, 3\pi/8, \pi/4, \pi/8, 0, \pi/8, \pi/4, \pi/2, 3\pi/4]$. The drag reduction in the subsampled resolvent model and the DNS was calculated for each case. The raw DR data were subsequently interpolated using bilinear splines and normalized with the respective maximum DR.

The resulting map of drag reduction as a function of y_d and $\angle A_d$ is shown in Figure 14, where Figure 14a is the resolvent model prediction and Figure 14b shows the DNS results. Each map is normalized by its maximum DR, which corresponds to 5% (resolvent model) and 21% (DNS), respectively. Bright shading (positive numbers) represent drag reduction, while dark colors (negative numbers) indicate drag increase. The solid black lines outline a few selected contour levels and the contour lines of Figure 14a are replotted as dotted blue lines in Figure 14b to facilitate comparison between resolvent model and DNS. Note that the contour levels of both plots are identical.

Figure 14b shows that the resolvent model is able to capture the trend observed in DNS over a wide range of parameters, but at a fraction of the cost. In terms of computational time, panels of Figure 14b took approximately 70 CPU hours on a laptop (resolvent model) and 4500 CPU hours on a computing cluster (DNS).

In both frameworks, the effect of the controller strongly depends on the phase shift $\angle A_d$ and generally speaking a small negative shift (e.g., $\angle A_d = /4$) leads to improved drag reduction, while a positive phase shift deteriorates the control performance and eventually leads to drag increase. Furthermore, both frameworks show that for a fixed positive phase shift $\angle A_d > 0$ the control performance decreases as y_d increases, while for a fixed negative phase shift $/2 < \angle A_d < 0$ the control performance initially increases, reaches a maximum, and then decreases as the sensor moves away from the wall. The qualitative agreement between the resolvent model and DNS can be made more clear by comparing the overlaid contour lines in Figure 14b. It is apparent that the contours of ξ of the resolvent model and the DNS collapse for $\angle A_d > 0$ over the entire range of y_d . This suggests that the model error between the resolvent approach and the DNS, reflected in the comparison of Reynolds stress profiles in Figure 13, is small with regards to the turbulent drag reduction *trends* for positive phase shifts. The model error in turbulent DR increases for more negative $\angle A_d$. However, the resolvent model is still able to capture the trend of the DNS reasonably well and also the parameter combination leading to maximum drag reduction is similar in both frameworks and corresponds to $y_d^+ \approx 1015$ and $\angle A_d \approx /4$. A formal representation of the model error is included in [31].

Our results suggest that resolvent analysis can provide a suitable flow model to design feedback flow control schemes for the purpose of drag reduction in incompressible wall-bounded turbulent flows even at technologically relevant Reynolds numbers.

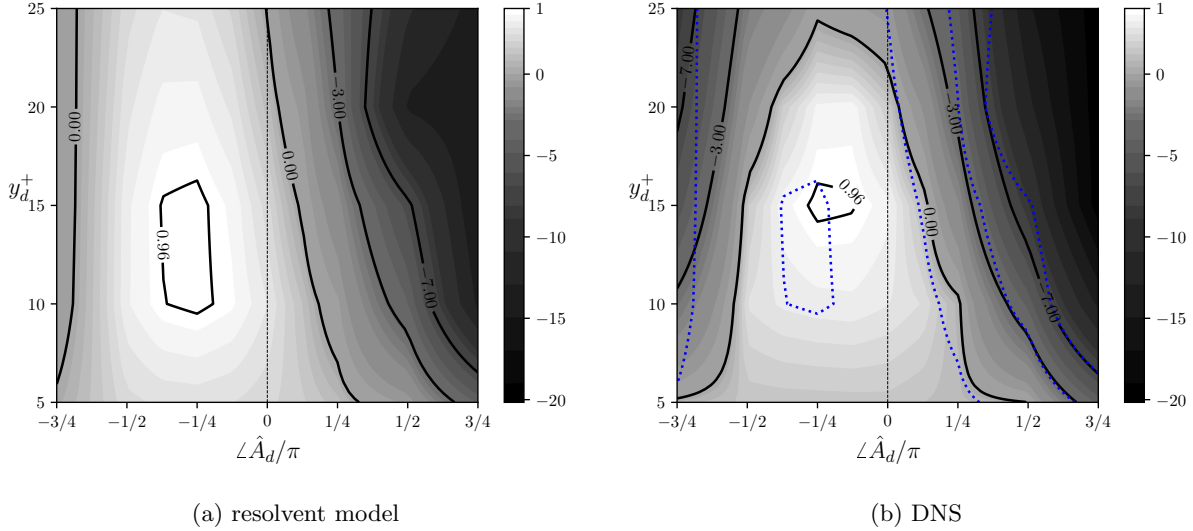


Figure 14: Contour map showing the drag reduction as a function of sensor location y_d^+ and phase shift $\angle A_d$. Figure (a) shows the prediction of the resolvent model, figure (b) displays DNS data, both contour maps are normalized with the respective maximum DR. The vertical dashed black line denotes opposition control ($\angle A_d = 0$) and the contour lines of figure (a) are replotted as dotted blue lines in figure (b).

3.3.4 Low-order models of linear and nonlinear effects in wall turbulence

McMullen, R., Rosenberg, K. & McKeon, B. J. Interaction of Orr-Sommerfeld and Squire modes in a low-order model of turbulent channel flow (In preparation.)

The results presented herein have several important implications for equation-driven modeling of turbulent channel flow. The first is that partitioning the resolvent operator into Orr-Sommerfeld and Squire subsystems, originally presented in the context of ECS [8], is also advantageous in terms of its ability to develop compact representations of fully turbulent channel flow at high Reynolds number. Furthermore, it provides valuable insight into the complex dynamics by identifying the competition mechanism between the OS and SQ modes, which has ramifications for modeling nonlinear interactions. Specifically, considering that for large Re , the OS singular values in the logarithmic and outer regions of the flow are much larger than the SQ ones, it may be tempting from a modeling perspective to neglect the SQ family of modes. However, doing so does not take into account the relative scaling of the forcing terms \hat{g}_v and \hat{g}_η in 1 – it implicitly assumes they remain of the same order. The present results indicate that this is not the case. In fact, the scaling results of the weights for all of the classes can be summarized as $|\chi_j^{\text{SQ}}/\chi_j^{\text{OS}}| \sim \sigma_j^{\text{OS}}/\sigma_j^{\text{SQ}}$.

Though the absolute scalings of the weights were not determined, the present work can be considered a starting point to guide further modeling efforts toward quantifying nonlinear interactions in turbulent channel flow. For instance, it is particularly intriguing that the v statistics depend only on the OS modes. Consequently, if the scaling of the OS weights can be determined from these, empirically or otherwise, then the results given above can be used to determine the scaling of the SQ weights, effectively reducing the number of unknowns by half. Then a single computation at a relatively low Reynolds number could be combined with the scalings to make predictions of the spectra at Reynolds numbers that are currently unattainable by simulations.

Taken together, the results point to the competition between the OS and SQ modes being an important mechanism in turbulent channel flow that should be respected in order to accurately model the statistics. We hypothesize that if this mechanism could be interrupted, the dynamics, and consequently the statistics, of the system would be significantly different. This line of inquiry is the subject of ongoing work.

3.4 Review articles

The support of this grant enabled the PI to contribute to three review articles related to the work under this and previous AFOSR grants.

1. The PI wrote the second ever (invited) *Perspectives* article in the Journal of Fluid Mechanics [5]. This article provided a pedagogical review of the origins and development of resolvent analysis for wall turbulence.
2. Our review of the use of dynamic roughness for manipulation of turbulent boundary layers [22] appeared in a special issue of the AIAA Journal on Flow Control.
3. The PI contributed to the section on Resolvent Analysis in a multi-author review on Modal Decompositions in fluid mechanics [4].

4 Conclusions and Outlook

This grant enabled progress to be made in the understanding of the flow physics underlying wall turbulence, and in particular the efficiencies associated with a spatio-temporal representation of the equations of motion, embodied in the low-rank characteristics of the resolvent operator and the limitations on the permitted nonlinear interactions between resolvent modes.

In particular, we have demonstrated that a significant reduction in degrees of freedom required to represent turbulent channel flow can be obtained using an Orr-Sommerfeld/Squire approach to resolvent analysis, and that further exploitation of self-similarity will be possible in the pursuit of low-order models of self-sustaining turbulent flows.

We have demonstrated the utility of the spatio-temporal formulation in describing nonlinear interactions in both computational and experimental settings, exploiting dynamic roughness actuation in the latter to generate synthetic turbulence.

We propose that the resolvent formulation is a useful tool by which to test control strategies at a significantly reduced cost: before expensive DNS studies or experiments are commissioned to investigate a particular approach, resolvent analysis can (or even should) be used to identify broad trends and locally optimal configurations.

Lastly, we have identified several results which will feature in ongoing efforts to develop low-order models of self-sustaining wall turbulence using resolvent analysis to describe the important linear and nonlinear phenomena involved.

5 Archival products under this grant

1. Symon, S., Rosenberg, K., Dawson, S. T. M. & McKeon, B. J. Non-normality and classification of amplification mechanisms associated with turbulent mean flows *Phys. Rev. Fluids*, 3(5), 053902 (2018) [29]
2. Rosenberg, K. & McKeon, B. J. Efficient representations of exact coherent states of the Navier-Stokes equations using resolvent analysis *Fluid Dyn. Res.*, 51, 011401 (2019)
3. McKeon, B. J., Jacobi, I. & Duvvuri, S. Dynamic roughness for manipulation and control of turbulent boundary layers: a review. *AIAA J.*, 56(6), 2178-2193 (2018) [22]
4. Taira, K., Brunton, S. L., Dawson, S. T., Rowley, C. W., Colonius, T., McKeon, B. J., Schmidt, O., Gordeyev, S., Theofilis, V. & Ukeiley, L. S. Modal analysis of fluid flows *AIAA J.*, 55(12), 4013-4041(2017). <http://arc.aiaa.org/doi/abs/10.2514/1.J056060> [4]
5. Jacobi, I. & McKeon, B. J. Phase relationships between scales in the perturbed turbulent boundary layer *J. Turb* 18(12), 1120-1143 (2017) [30]
6. Saxton-Fox, T. & McKeon, B. J. Coherent structures, uniform momentum zones and the streamwise energy spectrum in wall-bounded turbulent flows *J. Fluid Mech.*, 826, R6, 1-12 (2017) [24]
7. McKeon, B. J. The engine behind (wall) turbulence: perspectives on scale interactions *J. Fluid Mech. (Perspectives)*, 817, P1 (2017) [5]
8. Symon, S., Sipp, D. Schmid, P. & McKeon, B. J. Mean and unsteady flow reconstruction using data-assimilation and resolvent analysis *AIAA J.* (to appear, <https://doi.org/10.2514/1.J057889>)
9. Toedtli, S., Luhar, M. & McKeon, B. J. Predicting the response of turbulent channel flow to varying-phase opposition control: Resolvent analysis as a tool for flow control design *Phys. Rev. Fluids*, 4(7), 073905 (2019) [31]
10. Rosenberg, K. & McKeon, B. J. Computing exact coherent states in channels starting from the laminar profile: a resolvent-based approach *Phys. Rev. E* 100(2), 021101(2019).
11. Huynh, D. P. & McKeon, B. J. Characterization of the spatio-temporal response of a turbulent boundary layer to dynamic roughness *Flow, Turb. and Comb.* (to appear).
12. Huynh, D. P. & McKeon, B. J. Measurements of a turbulent boundary layer-compliant surface system in response to targeted, dynamic roughness forcing (Under review.)
13. Huynh, D. P. & McKeon, B. J. Resolvent analysis and experimental measurements on the effect of an elastic compliant wall on a dynamic roughness-forced turbulent boundary layer (In preparation.)
14. McMullen, R., Rosenberg, K. & McKeon, B. J. Interaction of Orr-Sommerfeld and Squire modes in a low-order model of turbulent channel flow (In preparation.)

6 References

- [1] B. J. McKeon and A. S. Sharma. A critical layer model for turbulent pipe flow. *J. Fluid Mech.*, 658:336–382, 2010.
- [2] P J Schmid and D S Henningson. *Stability and Transition in Shear Flows*. Springer-Verlag, New York, 2001.
- [3] R. Moarref, A. S. Sharma, J. A. Tropp, and B. J. McKeon. Model-based scaling and prediction of the streamwise energy intensity in high-Reynolds number turbulent channels. *J. Fluid Mech.*, 734:275–316, 2013.
- [4] K. Taira, S. L. Brunton, S. T. M. Dawson, C. W. Rowley, T. Colonius, B. J. McKeon, O. T. Schmidt, S. Gordeyev, V. Theofilis, and L. S. Ukeiley. Modal analysis of fluid flows: An overview. *AIAA J.*, 55(12):4013–4041, 2017.
- [5] B. J. McKeon. The engine behind (wall) turbulence: Perspectives on scale interactions. *J. Fluid Mech.*, 817:P1, 2017.
- [6] R. Moarref, M. R. Jovanović, A. S. Sharma, J. A. Tropp, and B. J. McKeon. A low-order decomposition of turbulent channel flow via resolvent analysis and convex optimization. *Phys. Fluids*, 26(051701), 2014.
- [7] A. S. Sharma, R. Moarref, B. J. McKeon, J. S. Park, M. Graham, and A. P. Willis. Low-dimensional representations of exact coherent states of the Navier-Stokes equations from the resolvent model of wall turbulence. *Phys. Rev. E*, 93:021102(R), 2016.
- [8] K. Rosenberg and B. J. McKeon. Efficient representation of exact coherent states of the Navier-Stokes equations using resolvent analysis. *Fluid Dyn. Res.*, 51(011401), 2019.
- [9] K. Rosenberg. *Resolvent-based modeling of flows in a channel*. Ph.d., California Institute of Technology, 2018.
- [10] K. Rosenberg and B. J. McKeon. Computing exact coherent states in channels starting from the laminar profile: a resolvent-based approach. *Phys. Rev. E*, 100(2)(021101), 2019.
- [11] F. Waleffe. On a self-sustaining process in shear flows. *Phys. Fluids*, 9(4):883–900, 1997.
- [12] P. Hall and S. J. Sherwin. Streamwise vortices in shear flows: harbingers of transition and the skeleton of coherent structures. *J. Fluid Mech.*, 661:178–205, 2010.
- [13] Lee M. and R. D. Moser. The high-Reynolds-number asymptotic development of nonlinear equilibrium states in plane Couette flow. *J. Fluid Mech.*, 750:99, 2014.
- [14] J. LeHew, M. Guala, and B. J. McKeon. A study of the three-dimensional spectral energy distribution in a zero pressure gradient turbulent boundary layer. *Expts. in Fluids*, 51(4):997–1012, 2011.
- [15] Yongwei Huang and Daniel P Palomar. Rank-constrained separable semidefinite programming with applications to optimal beamforming. *IEEE Transactions on Signal Processing*, 58(2):664–678, 2009.
- [16] A. Towne, O. T. Schmidt, and T. Colonius. Spectral proper orthogonal decomposition and its relationship to dynamic mode decomposition and resolvent analysis. *J. Fluid Mech.*, 847:821–867, 2018.
- [17] A. S. Sharma, R. Moarref, and B. J. McKeon. Scaling and interaction of self-similar modes in models of high-Reynolds number wall turbulence. *Phil. Trans. Royal Soc. A*, 375(2089)(20160089), 2016.
- [18] R. Moarref, A. S. Sharma, J. A. Tropp, and B. J. McKeon. A foundation for analytical developments in the logarithmic region of turbulent channels. *ArXiv*, (1409.6047), 2014.
- [19] B. J. McKeon. Self-similar hierarchies and attached eddies. *Phys. Rev. Fluids*, 4(8):082601, 2019.

- [20] R. McMullen, K. Rosenberg, and B. J. McKeon. Interaction of Orr-Sommerfeld and Squire modes in a low-order model of turbulent channel flow. *In preparation*.
- [21] S. Duvvuri and B. J. McKeon. Phase relations in a forced turbulent boundary layer: implications for modeling of high Reynolds number wall turbulence. *Phil. Trans. Royal Soc. A*, 375(2089)(20160080), 2017.
- [22] B. J. McKeon, I. Jacobi, and S. Duvvuri. Dynamic roughness for manipulation and control of turbulent boundary layers: An overview. *AIAA J.*, 56(6):2178–2193, 2018.
- [23] S. Duvvuri and B. J. McKeon. Non-linear interactions isolated through scale synthesis in experimental wall turbulence. *Phys. Rev. Fluids*, 1(3):032401(R), 2016.
- [24] T. Saxton-Fox and B. J. McKeon. Coherent structures, uniform momentum zones and the streamwise energy spectrum in wall-bounded turbulent flows. *J. Fluid Mech.*, 826(R6), 2017.
- [25] C.M. de Silva, N. Hutchins, and I. Marusic. Uniform momentum zones in turbulent boundary layers. *J. Fluid Mech.*, 786:309–331, 2016.
- [26] A. S. Sharma and B. J. McKeon. On coherent structure in wall turbulence. *J. Fluid Mech.*, 728:196–238, 2013.
- [27] M. Luhar, A. S. Sharma, and B. J. McKeon. Opposition control within the resolvent analysis framework. *J. Fluid Mech.*, 749:597–626, 2014.
- [28] Lee M. and R. D. Moser. Direct numerical simulation of turbulent channel flow up to $Re_\tau \approx 5200$. *J. Fluid Mech.*, 774:395, 2015.
- [29] S. S. Todtli, M. Luhar, and B. J. McKeon. Predicting the response of turbulent channel flow to varying-phase opposition control: resolvent analysis as a tool for flow control design. *Phys. Rev. Fluids*, 4(7):073905, 2019.
- [30] S. Symon, K. Rosenberg, S. T. M. Dawson, and B. J. McKeon. Non-normality and classification of amplification mechanisms in stability and resolvent analysis. *Phys. Rev. Fluids*, 3(053902), 2018.
- [31] I. Jacobi and B. J. McKeon. Phase-relationships between scales in the perturbed turbulent boundary layer. *J. Turb.*, pages 1–24, 2017.